RESEARCH ON THE MECHANISM AND PARAMETER OPTIMIZATION OF STRATIFIED SCREENING OF MILLET THRESHING MIXTURE BASED ON BRAZIL NUT EFFECT

/

基于巴西果效应的谷子脱出物分层筛分机理与参数优化研究

Dong-ming ZHANG[1)], Yi-fu CHEN[1)], Shu-juan YI*[1)], Song WANG[1)], Zi-yang HUANG[1)]
College of Engineering, Heilongjiang Bayi Agricultural University, Daqing/P. R. China
Tel: +86-459-13836961877; E-mail: yishujuan_2005@126.com;
Corresponding author: Shu-juan Yi
DOI: https://doi.org/10.35633/inmateh-77-24

Keywords: *millet threshing mixture; cleaning; Brazil Nut Effect; parameter optimization; wrapping loss*

ABSTRACT

To address the challenges of millet threshing mixtures, namely their light mass, small volume, minimal differences in component suspension speeds, and susceptibility to interference from impurities during sorting, which lead to high loss and impurity rates, this study applies the Brazil Nut Effect (BNE) to optimize the operating parameters of an air-sieve-type grain sorting device. The discrete element method (DEM) was used to numerically simulate the sieving and segregation processes of the millet threshing mixture, to clarify the grain population structure most conducive to effective sieving, and to identify the main factors influencing segregation and stratification as well as the appropriate parameter ranges. A bench-scale multifactor performance test was conducted to establish regression equations describing the effects of amplitude, stepped jitter plate length, crank rotational speed, and fan shaft rotational speed on loss rate and impurity rate. Using a multi-objective optimization method, the optimal parameter combination was determined as follows: amplitude of 26 mm, stepped jitter plate length of 450 mm, crank rotational speed of 580 rpm, and fan shaft rotational speed of 645 rpm. Under these conditions, the loss rate was 2.68% (with coiling loss below 0.5%) and the impurity rate was 3.95%. The results of this study provide a reference for optimizing the operating parameters of millet cleaning devices.

摘要

针对谷子籽粒质量轻、体积小、脱出物各成分悬浮速度差异小，清选时籽粒易受杂余裹挟，造成损失与含杂率高等问题，本研究基于巴西果效应对风筛式谷子清选装置作业参数进行优化。采用离散元方法对谷子脱出物透筛、离析过程进行数值模拟，明确最有利于籽粒透筛的粒群结构，得到影响离析分层的主要因素和参数选择范围。进行了台架多因素性能试验，建立振幅、抖动板长度、曲柄转速、风机轴转速对损失率、含杂率建立回归方程，并利用多目标优化方法获取最优参数组合为：振幅 26mm、抖动板长度 450mm、曲柄转速 580r/min、风机轴转速 645r/min，在此参数组合下，损失率为 2.68%，其中裹挟损失小于 0.5%，含杂率为 3.95%。研究结果为谷子清选装置参数优化提供了参考。

INTRODUCTION

As a small-seeded grain with omnivorous dietary characteristics, millet is rich in dietary fiber and various nutrients, serving as an important supplement to the nutritional structure of staple grains and occupying a significant position in China's grain market (*Liu et al., 2022; Guo et al., 2021*). Cleaning is a key stage in the millet harvesting process, as it directly affects harvest losses and impurity content, and is therefore a critical factor in ensuring grain quality and yield (*Wang et al., 2014; Wang et al., 2021; Liu et al., 2019; Wang et al., 2025*). The millet threshing mixture is composed of kernels, millet panicle clusters, stalks, and light miscellaneous residues (e.g., prickly hairs, chaff). Due to the low mass of millet kernels and the complex composition of the mixture, the airflow distribution during cleaning can be easily disturbed, leading to increased grain loss and impurity content. Similar issues of airflow disturbance and separation inefficiency in cereal cleaning devices have also been reported in related studies (*Mircea et al., 2020; Vladut et al., 2022*). Compared with rice, corn and other staple crops, the degree of mechanization of millet harvesting is still insufficient, and there is an urgent need to carry out systematic research on the problems of cleaning loss and impurity.

[1] *Dong-ming Zhang, Ph.D.; Yi-fu Chen, M.Sc.; Shu-juan Yi, Prof. Ph.D.; Song Wang, Ph.D.; Zi-yang Huang, M.Sc.*

In recent years, domestic research on multi-crop joint harvesting cleaning devices has continued to deepen. Many scholars have conducted extensive exploratory studies on the structural optimization and key functional components of such devices, promoting technological progress and improving the adaptability of cleaning equipment. *Kang Jiaxin et al. (2025)* designed an independently adjustable concave plate sieve device and verified its effectiveness in improving the performance and adaptability of sorting through multi-crop tests. *Wang Fanrui et al. (2024)* designed an air-screen type cleaning device for cumin cleaning problems and optimized it through gas-solid coupling simulation and test, which significantly improved the cleaning efficiency and accuracy. *Bao Guocheng et al. (2024)* designed a wing-type curved surface debris removal device based on the airflow Kanda effect and verified the feasibility of its function of separating the light impurities in the corn detritus mixture. *Wang Fei et al. (2024)* designed a corn cleaning device with pre-cleaning function, which further optimized the quality of large-feed corn cleaning operation. *Hud et al. (2023)* demonstrated that the use of a multi-purpose screw conveyor-separator can significantly enhance the separation efficiency of agricultural materials, highlighting the potential of structural innovations in improving cleaning and sorting performance. In addition, the crop cleaning process is essentially a complex multi-component particle motion coupled with sieving behavior, and the size, density and shape differences of particles are the fundamental driving force for the changes in their distribution (*Jiang et al., 2023*). Previous studies have demonstrated that vibration- or airflow-induced relative motion among particles contributes to the formation of stratified structures, which in turn influence the penetration trajectory and efficiency of particles through the sieve (*Cristea et al., 2023; Vladuț et al., 2023*). Other researchers have focused on modeling and contact parameter calibration of dislodged particles in order to enhance the accuracy of simulated particle motion behavior (*Guo et al., 2024; Li et al., 2025*). In summary, a number of studies have achieved certain research results in the optimization of the structure of the cleaning device, the design of key components, particle dynamics modeling and simulation analysis, etc. However, there are fewer studies related to the cleaning device in the millet combined harvesting, especially in the mechanism of the cleaning behavior of the small particle size, light weight, multi-component materials under the conditions of the key structural adaptability of the cleaning behavior mechanism, but there is a lack of systematic and in-depth theoretical and practical explorations.

In this paper, a model of particle movement and segregation of the millet threshing mixture on the vibrating screen surface was constructed based on the principle of the Brazil Nut Effect. The layered structural features conducive to improving the efficiency of grain sieve penetration were proposed. A four-factor, five-level quadratic rotary orthogonal combination experiment was designed to optimize the key operating parameters of the air-sieve cleaning device, thereby systematically evaluating the applicability and regulatory potential of the Brazil Nut Effect in cleaning and loss reduction. The study aims to reduce the loss rate and impurity rate during the millet cleaning process and to provide theoretical support and a technical pathway for the efficient cleaning of small-grain crops.

MATERIALS AND METHODS

Structure and working principle of the cleaning device

The air-sieve cleaning device is mainly composed of a vibrating screen, a fan, a tailing auger, and a grain auger. Specifically, the vibrating screen includes a stepped jitter plate, top sieve, bottom sieve, and tail sieve, while the fan consists of a rotor, blades, and air guide board. The overall structure of the device, measuring 1695 mm in length and 1085 mm in width, is shown in Fig. 1.

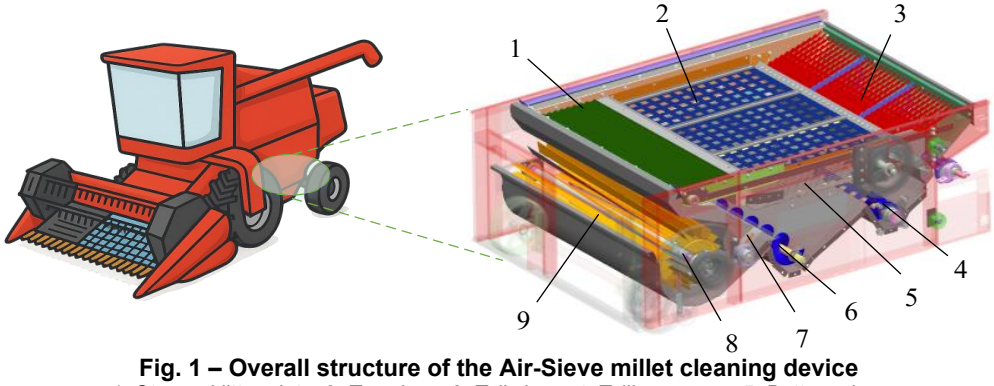

Fig. 1 – Overall structure of the Air-Sieve millet cleaning device

1. Stepped jitter plate; 2. Top sieve; 3. Tail sieve; 4. Tailings auger; 5. Bottom sieve 6. Grain auger; 7. Air guide board; 8. Fan rotor; 9. Fan Blades

The air-sieve-type millet cleaning device integrates air separation and screening, making full use of the geometric characteristics of the discharged material and the differences in suspension behavior among its components to achieve efficient separation of grains and impurities. During the cleaning process, a large amount of millet threshing mixture accumulates on the vibrating screen at the front end of the stepped jitter plate. Driven by the vibration of the plate, the mixture moves axially toward the rear end of the vibrating screen, where air-sieving and screening act together to separate the grains from millet panicle clusters and stalks. The panicle clusters are directed into the re-threshing agitator and conveyed by its screw to the threshing and separating unit for repeated threshing. Short stalks and light impurities are discharged from the device through the tail-end outlet. Due to the small size and low mass of millet kernels, they are more susceptible to airflow disturbances, making millet cleaning more challenging than that of larger-seeded crops. In particular, during the separation process, the grains are easily entrained by stalks and debris, leading to increased grain loss.

Millet threshing mixture

The millet threshing mixture is the product of the threshing and separation process and serves as the primary material for the cleaning stage. Determining its composition and characteristics forms the basis for theoretical and simulation analyses. The mixture mainly consists of grains, millet panicle clusters, short stalks, and light residues (such as bristles and husks). Due to the small volume and mass of the light residues, their influence on the sieving process can be neglected. The millet threshing mixture and its components are shown in Fig. 2.

Fig. 2 – Main components of millet threshing materials

Discrete element method and modeling

Discrete Element Method (DEM) is a numerical computational method based on the principle of particle dynamics, which can be used to simulate the movement laws among microscopic individuals and the macroscopic collective behaviors in the particle system. It has been widely used in the study of transportation, mixing, separation and other processes of granular materials. The method considers particles as independent discrete bodies, and dynamically tracks their motion, collision and energy transfer processes under external forces by solving the Newton-Euler equations of motion and combining with the calculation of contact forces and moments between particles. In the simulation process, a reasonable contact model plays a key role in the accurate reproduction of particle behavior. In view of the diverse morphology and complex interaction of the particles in millet threshing mixture, the Hertz-Mindlin contact model is chosen to model the contact-collision behavior in this paper. The model is suitable for describing the interaction between particles characterized by elastic deformation, frictional slip and nonlinear contact stiffness. It can more realistically reflect the mechanical response of the particles in the millet clearing process.

In order to deeply analyze the relationship between dissociative sieving and grain clearing quality, firstly, the simulation analysis of grain threshing mixture through sieving was carried out to obtain the particle structure which is favorable for grain sieving, and then the simulation analysis of grain threshing mixture through dissociative sieving was carried out to obtain the main factors and the range of values which affect the dissociative stratification of the grains. Therefore, discrete element method for modeling of millet threshing mixture, modeling of sieve permeability, and modeling of segregation were carried out respectively.

To deeply analyze the relationship between the dissociation sieve and the quality of grain cleaning, a simulation analysis of the millet threshing mixture during sieving was first conducted to identify the particle structure most favorable for grain penetration through the sieve. Then, the simulation analysis of grain threshing mixture dissociation was carried out to obtain the main factors and the range of values affecting the

particle dissociation stratification. Therefore, discrete element method of millet threshing mixture modeling, sieve permeability modeling, and segregation modeling were carried out respectively. The millet threshing mixture contains a large number and proportion of grains, which exhibit relatively high sphericity. Therefore, each grain was modeled as a single spherical particle with a radius of 0.75 mm. The millet panicle clusters are filled according to the standard sphere, rectangle, cone, and ellipsoid, which are automatically filled by setting the parameters of spherical filling accuracy, smoothness, and the number of spherical surfaces. According to the size distribution data of the millet clusters, the length L=8mm is taken as the benchmark, and the four standard body contours are established for automatic filling to form the benchmark millet clusters particles. For the millet panicle clusters within the range of length 3mm ≤ L ≤ 13mm and L ≠ 8mm, the benchmark millet panicle can be scaled according to the ratio. The short stalks are arranged in a straight line with spherical surfaces to form cylinder-like spherical surfaces with a radius of 1mm and a sphere center interval of 1 mm. The size of the grain can be adjusted by setting the number of filled spherical surfaces and the scaling of the grains. The final particle model of grains, millet panicle clusters and short stalks is shown in Fig. 3.

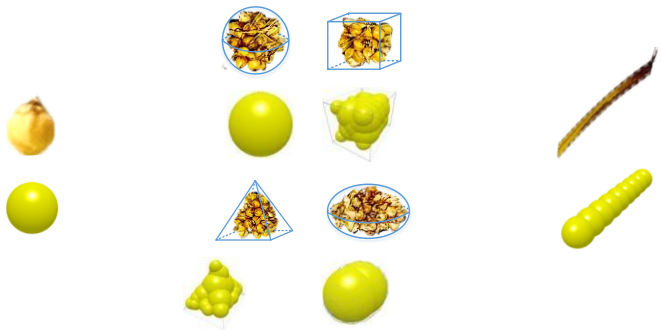

(a) Grain (b) Millet panicle cluster (c) Short stalks

Fig. 3 – Discrete element model of millet threshing materials

Reasonable and accurate particle parameter setting in discrete element method is an important factor that affects the simulation results. The material of stepped jitter plate and vibrating screen in contact with millet threshing mixture particles in EDEM simulation is steel 45. The simulation related material intrinsic parameters and contact parameter settings are shown in Table 1 and Table 2.

Table 1

Intrinsic parameter settings

Components of millet threshing materials	Poisson's ratio	Shear modulus / Mpa	Density / (kg.m^{-3})
Grains	0.39	1.46	1200
Millet panicle cluster	0.36	0.42	800
Short stalks	0.25	1.44	300
Steel 45	0.28	2.09×10^{5}	7850

Table 2

Contact parameter settings

Components of millet threshing materials	Poisson's ratio	Shear modulus / Mpa	Density / (kg.m^{-3})
Grains-grains	0.55	0.03	0.39
Millet panicle cluster-millet petals	0.71	0.05	0.28
Short stalks-short stalks	0.60	0.04	0.39
Grains-millet petals	0.52	0.04	0.30
Grains-short stalks	0.58	0.03	0.36
Millet panicle cluster-short stalks	0.65	0.04	0.30
Grains-Steel 45	0.56	0.04	0.45
Millet panicle cluster-Steel 45	0.59	0.03	0.32
Short stalks-Steel 45	0.61	0.02	0.41

The simulation model of millet threshing mixture sieve penetration was established, as shown in Fig. 4. The sieve used in the model is a flat square-hole sieve with 8 × 8 mm openings. The grain layer is placed on top of the sieve, with two baffles positioned above the sieve and at the bottom of the model, respectively. In order to avoid the influence of sidewalls on the particle motion, Periodic Boundary Conditions (PBC) were set for the x-z and y-z directions of the computational domain (*Dubey et al., 2024*). Taking the x-z direction as an example, any particle leaving the boundary in the *y* direction will return to the computational domain from the -y direction.

The PBC setting enables the model to simulate the global state through local simulation, which reduces the amount of simulation operations and ensures the accuracy of the simulation at the same time. The three-axis dimensions of the model's computational domain should all be larger than 20 times the minimum particle diameter, so the sieve body is set up with four sieve holes in both x and y directions according to the smallest square area that can be intercepted to meet the local simulation accuracy requirements (*Hou et al., 2022*).

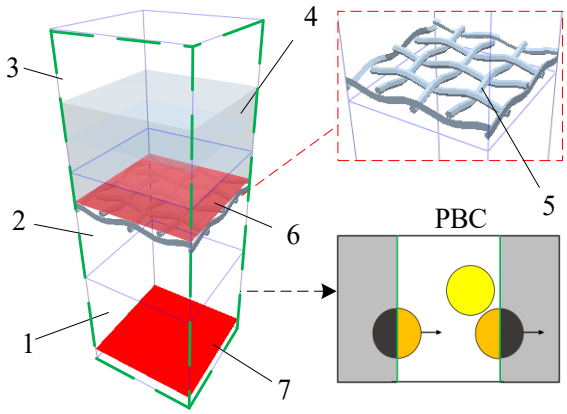

Fig. 4 - Screening model

1. Mesh a; 2. Mesh b; 3. Mesh c; 4. Particle factory; 5. Sieve; 6. Flap a; 7. Flap b

The particle parameters were defined as follows: grain particles were modeled as spherical particles with a diameter of Φ 1.5 mm, millet cluster particles as spherical particles with a diameter of Φ 6 mm, and short-stalk particles as cylindrical particles with a diameter of Φ 2 mm and a length of 10 mm. According to the mass ratios reported by *Wang F. et al (2024),* the generation quantity ratio of grains, millet clusters, and short stalks was set to 80:1:2. To clarify the influence of particle-bed structure on the sieve-through process, the three types of millet threshing mixture particles were arranged in different stratified configurations to construct six idealized particle structure models, denoted as a - f, as shown in Fig. 9. The simulation procedure was as follows: the layered particles were first generated and kept stationary on baffle plate A to allow the system to reach a stable state; then, baffle plate A was removed, and vibration was applied to the sieve body along the z-axis with an amplitude of 20 mm and a frequency of 7 Hz. The simulation was terminated once all grains had passed through the sieve.

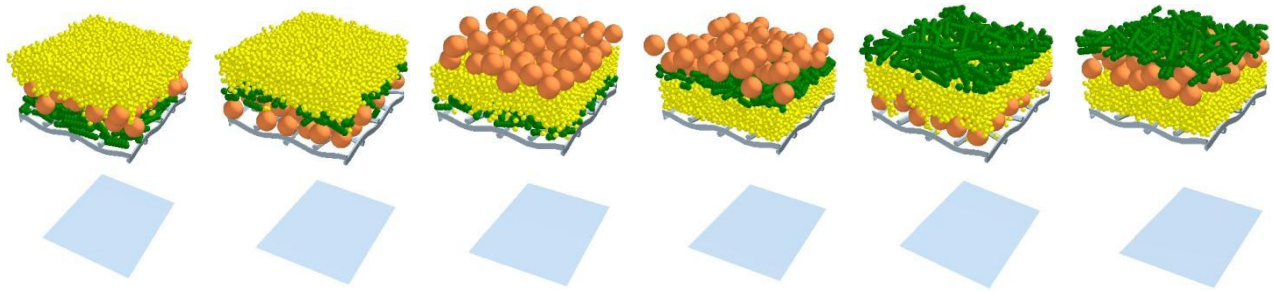

(a)Model a (b)Model b (c)Model c (d)Model d (e)Model e (f)Model f

Fig. 5 - Ideal Particle Layering Model

The segregation model of the millet threshing mixture was constructed, and its simulation domain is shown in Fig. 6(a). To minimize the convection phenomena caused by collisions and friction between particles and the sidewalls, periodic boundary conditions (PBC) were applied in both the x-z and y-z directions. The bottom surface of the model is a square plane with a side length of 30 mm. The vibration mode adopts one-dimensional simple harmonic motion along the z-axis.

For the simulation, a single large particle representing a millet panicle or stalk was first generated and placed at the bottom of the model. Subsequently, a number of small grain particles were generated until the total height of the particle system reached 20 times the grain diameter, corresponding to approximately 45 mm. Once the particle system reached a stable state, as shown in Fig. 6(b), the process of large-particle migration was observed, and the vertical coordinates of the large particles were recorded. When the large particles reached the surface of the granular system, the planar vibration was stopped.

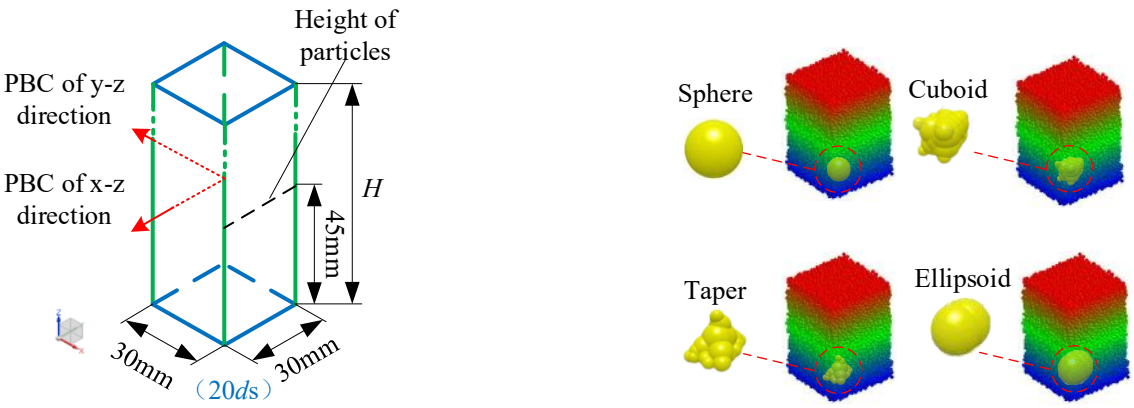

(a)Computational domain (b)Initial state of dissociation simulation

Fig. 6 - Segregation model

RESULTS AND DISCUSSIONS

Analysis of the simulation results of the screening model

To better capture the differences in the motion characteristics of various particle structure models on the sieve, DEM simulations of sieve penetration were conducted for six idealized particle structure models, labeled a–f. When grains enter the grid region a, it can be regarded as the effective sieve-penetration zone. The simulation post-processing function was used to record the change in the number of grains passing through grid a over time for each of the six simulation groups. The resulting curves are shown in Fig. 7.

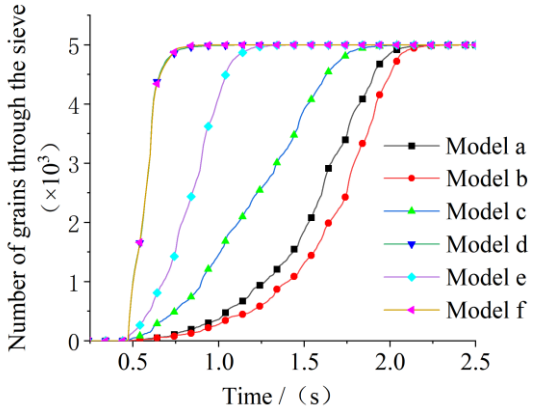

Fig. 7 - Time variation curve of grain passing through the sieve

From the simulation analysis of the sieve-penetration process, it can be seen that the sieve-penetration rate of grain particles varies significantly among different particle-structure models. The total times required for all grains to pass completely through the sieve in models a–f were 2.5 s, 2.5 s, 2.3 s, 1.21 s, 1.47 s, and 1.2 s, respectively. In models d and f, where the grains were positioned in the bottom layer, the total sieve-penetration time was approximately half that of the top-layer configurations in models a and b. For the sieving rate analysis under uniform grain fall, the number of particles passing through the sieve was taken to vary linearly within the steady sieving stage. The initial and final time intervals for this stage were 0.47-2.03 s, 0.47-2.09 s, 0.47-1.78 s, 0.47-0.65 s, 0.47-1.12 s, and 0.47-0.65 s, respectively, for models a–f. The data from the six groups were linearly fitted using the Origin analytical software, yielding slope values of 3.32, 2.90, 4.16, 24.77, 8.36, and 24.58, respectively. These results indicate that, under the experimental conditions of this study, the grain sieving rate in models with grains located in the bottom permeable layer is significantly higher than in the other configurations.

From the above analysis, there is a significant difference in the sieving rate of grains under different particle structures; therefore, models a and f were selected for further investigation to identify the causes of these differences. As shown in Fig. 8, the sieving process can be divided into three stages: *free fall*, *collision*, and *compression*. In model a, where the grains are located in the top layer, they must pass through the millet panicle cluster and stalk layers before reaching the sieve. When the particles at the bottom of the model collide with the sieve surface, local blockages form due to interlocking effects.

Consequently, a large number of millet panicle cluster and stalk particles move upward with the vibrating sieve, forcing the grains to move upward as well. The direction of the force acting on the grains is opposite to the motion of the sieve body, resulting in only a small number of grains passing through the sieve during the collision and compression stages. In contrast, in model f, the grains are positioned in the lowest layer and can pass directly through the sieve. The millet panicle cluster and stalk particles above the grains, driven by inertia, help accelerate the grains downward and prevent them from rebounding upward. In this case, the direction of the force acting on the grains coincides with the motion of the sieve body. In summary, when the grains are located in the bottom layer of the particle structure, the sieving rate is significantly improved.

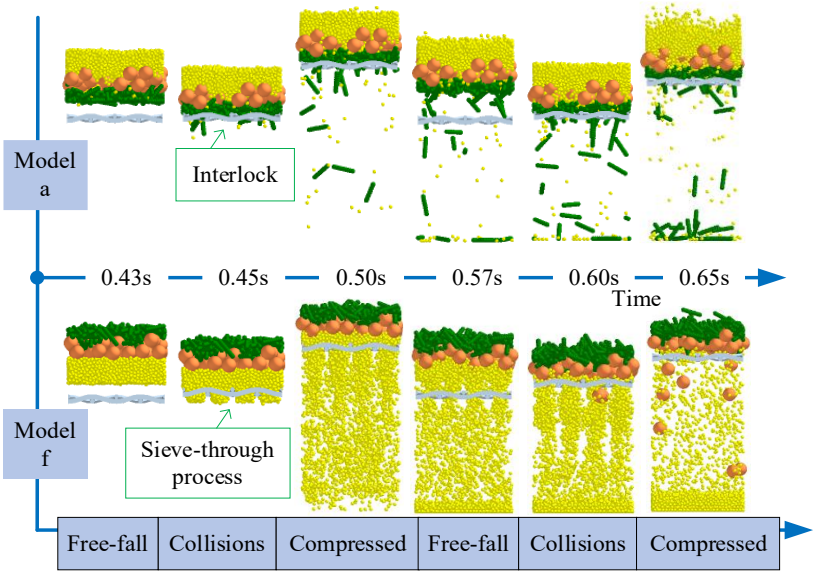

Fig. 8 - Simulation of the screening process

Analysis of the simulation results of the segregation model

Under planar vibration at 7 Hz and 20 mm amplitude, dissociation simulations were performed for four large-particle shapes representing millet panicle clusters. The temporal evolution of the large particles' vertical position was analyzed, with results plotted in Fig. 9: the x-axis denotes simulation time, the z-axis the vertical height of the large particle, and the y-axis represents the shape of millet panicle cluster. Numerical height recording stopped once a large particle reached the free surface of the granular bed. To keep data vectors equal in length for processing, the remaining samples after dissociation were padded with zeros, causing the z-axis trace to coincide with the x-axis following completion of segregation. Consequently, the length of the terminal straight segment serves as an inverse indicator of dissociation time: the longer this flat segment, the shorter the dissociation time.

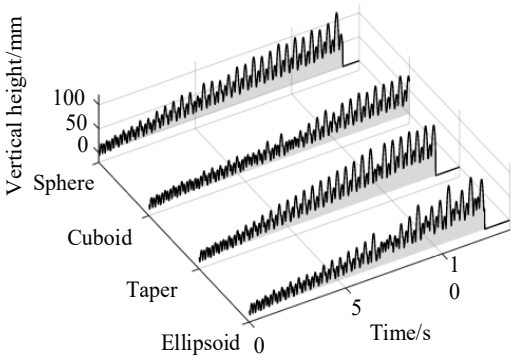

Fig. 9 - Effect of shape on millet panicle cluster segregation process

The results show that all four shapes of millet panicle particles exhibited the "Brazil Nut" segregation pattern, in which the large panicle cluster particles migrated to the top of the granular system. The average segregation times for the spherical, rectangular, conical, and ellipsoidal particles were 12.36 s, 12.05 s, 13.70 s, and 13.14 s, respectively. Although the dissociation rate of the conical particles was relatively slow, a comprehensive analysis of both the segregation pattern and segregation time indicates that particle shape has a limited influence on the segregation behavior of millet panicle clusters.

A plane vibration frequency of 7 Hz was used to investigate the influence of vibration amplitude on the segregation behavior of spherical grain particles. The amplitude range was set between 10 and 35 mm, with a step size of 5 mm. The time-amplitude-vertical height curves are shown in Fig. 10(a). When the amplitude was 10 mm, the millet panicle clusters did not exhibit the “Brazil Nut” segregation pattern, and their relative positions remained near the bottom plane throughout the simulation. When the amplitude increased from 15 to 35 mm, the millet panicle clusters exhibited a clear “Brazil Nut” segregation pattern. As the amplitude increased from 15 mm to 30 mm, the segregation time increased slightly; however, when the amplitude reached 35 mm, the segregation time increased markedly. At this amplitude, the millet panicle clusters had already reached the upper layer of the particle system within 8–11 s of simulation. During this period, the clusters vibrated intensely due to the bottom-plane excitation, reaching a peak vertical height of 286.6 mm. Between 11 and 16 s, the vibration amplitude of the clusters gradually decreased, indicating that they had stabilized in the upper layer of the particle bed.

This indicates that the millet panicle clusters are located in the middle layer of the particle system. Overall, vibration amplitude has a notable influence on the disintegration behavior of millet panicle clusters. As the amplitude increases, the overall trend of segregation time also increases. A larger amplitude introduces higher system energy, causing more intense particle motion and reducing the stability of the segregation process. To further investigate the effect of vibration frequency on the segregation behavior of spherical millet panicle clusters, the vibration amplitude was fixed at 20 mm, and the vibration frequency was varied from 3 to 13 Hz in steps of 2 Hz. The time-frequency-vertical height curves are shown in Fig. 10(b). When the vibration frequency was 3 Hz or 5 Hz, the millet panicle clusters did not exhibit the “Brazil Nut” segregation pattern. However, at frequencies between 7 and 13 Hz, the “Brazil Nut” segregation pattern was clearly observed, and the segregation time decreased with increasing vibration frequency.

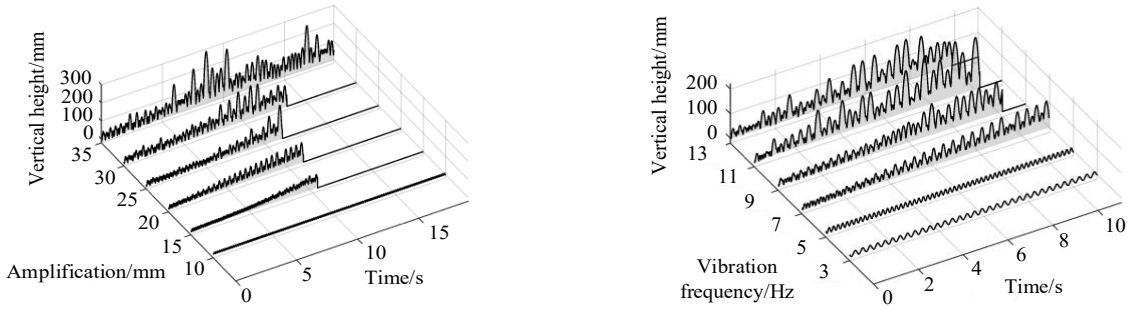

(a) Amplitude (b) Vibration frequency

Fig. 10 - Effect of vibration parameters on the process of millet panicle cluster segregation

Referring to the simulation tests of millet panicle clusters, the bottom-plane vibration amplitude and frequency were selected as the key parameters for the segregation simulation of stalk particles. As shown in Fig. 11(a), when the amplitude was 10 mm, the stalk particles did not exhibit the “Brazil Nut” segregation pattern. The variation in segregation time with amplitude showed no clear monotonic trend. As illustrated in Fig. 11(b), when the vibration frequency was 3 Hz or 5 Hz, the stalk particles did not exhibit the “Brazil Nut” segregation pattern. However, when the vibration frequency ranged from 7 to 13 Hz, the “Brazil Nut” segregation pattern was clearly observed. At a vibration frequency of 9 Hz, the segregation time decreased significantly, after which it showed only a slight further reduction.

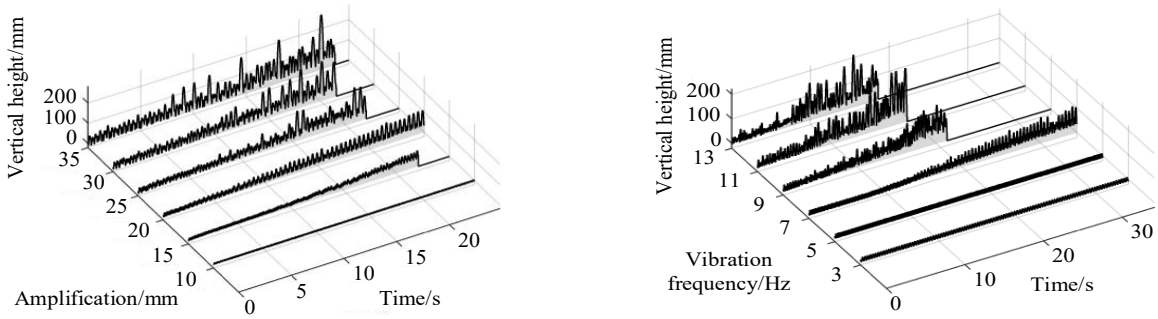

(a) Amplitude (b) Vibration frequency

Fig. 11 - Effect of vibration parameters on the process of stalks segregation

Segregation rate analysis

The dissociation rate is an important indicator of the reaction system subjected to the Brazil Nut Effect and was calculated according to Equation (1).

$$v_L = \frac{H}{t_L} \quad (1)$$

where: v_L is the dissociation rate, mm/s; H is the height of the dissociated model particle system, mm; and t_L is the average dissociation time, s.

The segregation rates of millet panicle clusters and stem particles in the segregation model were calculated for different amplitudes and vibration frequencies, and the curves were plotted as shown in Fig. 12. For the simulation test group that did not occur in the Brazil nut segregation mode, the segregation rate of large particles can be regarded as 0 mm/s and can be omitted. From the variation curve of segregation rate, it can be seen that the segregation rate of millet panicle clusters and stalk particles under different amplitudes and vibration frequencies is obviously different. And under the same conditions, the rate of the millet panicle cluster is higher than that of the stalks. From Fig. 12(a), it can be seen that with the increase of amplitude, the dissociation rate of millet panicle clusters showed a decreasing trend. When the amplitude is 15-25mm, the change is smooth. When the amplitude is greater than 25mm the millet panicle cluster segregation rate decreases significantly. As the vibration amplitude increased, the segregation rate of stalk particles first increased and then decreased, reaching its maximum value at an amplitude of 25 mm. As shown in Fig. 12(b), with increasing vibration frequency, the segregation rate of both millet panicle clusters and stalk particles initially increased and then gradually stabilized. When the vibration frequency exceeded 9 Hz, no significant change in the particle segregation rate was observed.

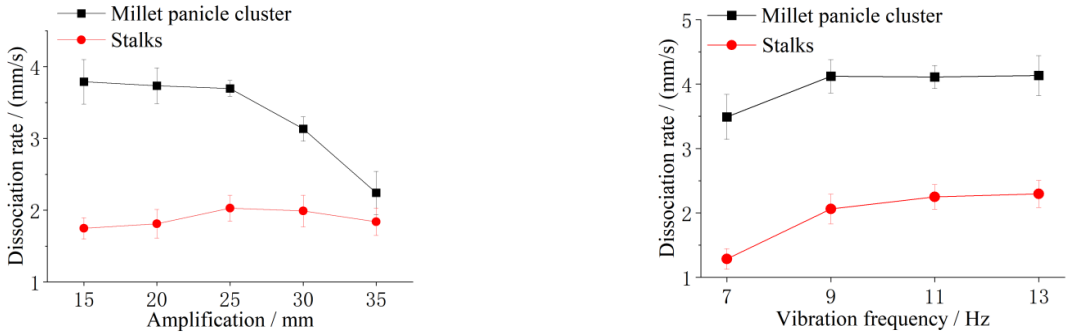

(a) Amplitude (b) Vibration frequency

Fig. 12 - Effect of amplitude and vibration frequency on segregation rate

Therefore, in the subsequent optimization test of the working parameters of millet threshing mixture, the amplitude range was selected from 15 to 35 mm, and the vibration frequency range was selected from 7 to 13 Hz. The middle value was finally taken as the zero level value.

Analysis of particle motion on stepped jitter plate

Simulation analysis showed that separation time is the key factor influencing particle stratification, and it is primarily determined by the length of the jitter plate. To determine the appropriate range of plate length, a three-dimensional model of the jitter plate was established using SOLIDWORKS and imported into EDEM for simulation and analysis of particle movement on the plate, as shown in Fig. 13. Data for individual particles were collected for analysis. The axial movement velocities of ten particles - grains, millet panicle clusters, and stalks - were calculated and averaged, yielding values of 77.6 mm/s, 50.2 mm/s, and 31.5 mm/s, respectively.

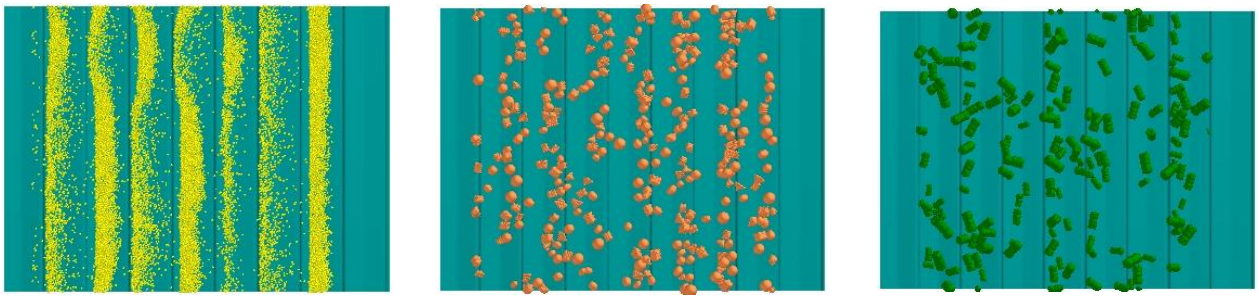

(a)Grain (b)Millet panicle cluster (c)Short stalks

Fig. 13 - Simulation of millet threshing material motion on the stepped jitter plate

The length of the stepped jitter plate is jointly determined with the average rate of axial movement of particles v_x, the thickness of the material H_w, and the rate of segregation v_L, which can be calculated by equation (2).

$$\begin{cases} L_d = v_x \cdot \dfrac{H_w}{v_L \cdot k} \\ k = \eta_A / \eta_0 \end{cases} \quad (2)$$

where: L_d is the length of the jitter plate, mm; v_x is the average rate of axial movement of particles, mm/s; H_w is the thickness of the material, mm; k is the correction coefficient; η_A is the actual porosity, %; and η_0 is the porosity of the simulation model, %.

The range of the length of the stepped jitter plate was calculated to be 197.80-638.22 mm. Therefore, the length of the stepped jitter plate was selected to be 200-640 mm.

Bench test

The experimental millet variety was selected as “Longgu 31”, and the experimental materials were taken from Zhaoyuan area, Daqing City, Heilongjiang Province, China. The millet threshing mixture was harvested, transported, threshed and separated. The experimental equipment is shown in Figure 14.

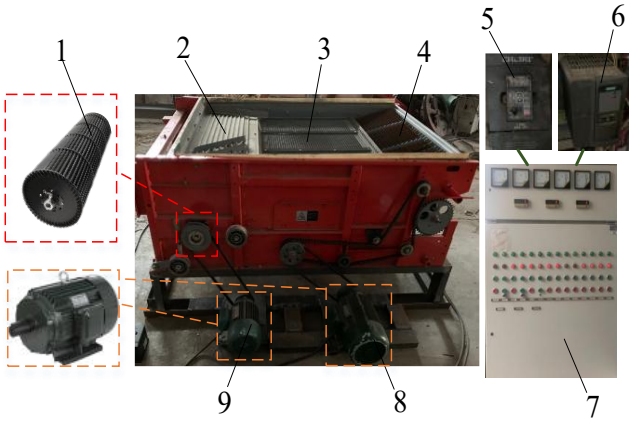

Fig. 14 - Millet air-sieve cleaning device test bench

1. Fan; 2. Stepped jitter plate; 3. Upper vibrating screen; 4. Tailing screen; 5. Fan shaft speed controller; 6. Crank speed controller; 7. Electrical control unit; 8. Vibrating screen crank drive motor; 9. Fan drive motor

Test Factors and Indicators

This study selects vibrating screen amplitude, stepped jitter plate length, crank speed and fan shaft speed as test factors to carry out experimental research on the performance of air sieve type millet cleaning device.

The grain loss rate and impurity content rate were selected as evaluation indicators and were calculated according to Equation (3).

$$\begin{cases} Y_1 = 1 - \dfrac{m_1}{m_2} \\ Y_2 = 1 - \dfrac{m_1}{m_3} \end{cases} \quad (3)$$

where: Y_1 is the grain loss rate, %; Y_2 is the grain impurity rate, %; m_1 is the mass of grain passing through the sieve, g; m_2 is the total mass of grain fed, g; m_3 is the total mass of sieve-through material, g.

Test results and analysis

Combining the results and analyses of the above dissociative sieve simulation tests, the Box-Behnken experimental design was adopted to determine the optimal operating parameters of the air-sieve grain cleaning device. The vibrating sieve amplitude (x_1), stepped jitter plate length (x_2), crank rotational speed (x_3), and fan shaft rotational speed (x_4) were selected as the independent variables, while the grain loss rate (y_1) and impurity rate (y_2) were taken as the dependent variables. A multifactor experiment was conducted to investigate the optimal operating parameters of the air-sieve-type millet cleaning device. The coding levels of each factor are shown in Table 3. The experimental design was generated using Design-Expert software, resulting in a total of 30 test groups, as shown in Table 4, where X_1, X_2, X_3, and X_4 represent the coded values.

Table 3

Test factor level table

Coding	Factor			
	Amplitude x_1(mm)	Plate length x_2(mm)	Crank speed x_3 (r·min^{-1})	Fan shaft speed x_4 (r·min^{-1})
-2	15	200	420	500
-1	20	310	510	600
0	25	420	600	700
1	30	530	690	800
2	35	640	780	900

Table 4

Test scheme and results

Number	Amplitude X_1	Plate length X_2	Crank speed X_3	Fan shaft speed X_4	Loss Rate Y_1(%)	Impurity rate Y_2(%)
1	-1	-1	-1	-1	11.82	21.53
2	1	-1	-1	-1	11.92	21.02
3	-1	1	-1	-1	10.94	9.35
4	1	1	-1	-1	5.99	8.6
5	-1	-1	1	-1	10.14	21.38
6	1	-1	1	-1	10.33	21.87
7	-1	1	1	-1	15.48	9.39
8	1	1	1	-1	12.74	9.6
9	-1	-1	-1	1	11.63	21.61
10	1	-1	-1	1	11.7	20.9
11	-1	1	-1	1	16.63	10.65
12	1	1	-1	1	13.78	9.52
13	-1	-1	1	1	14.83	24.15
14	1	-1	1	1	14.12	23.59
15	-1	1	1	1	27.47	13.2
16	1	1	1	1	23.54	11.62
17	-2	0	0	0	11.57	13.16
18	2	0	0	0	7.57	12.12
19	0	-2	0	0	21.75	38.78
20	0	2	0	0	25.4	15.53
21	0	0	-2	0	7.83	12.19
22	0	0	2	0	11.64	15.5
23	0	0	0	-2	3.74	7.69
24	0	0	0	2	10.48	11.14
25	0	0	0	0	2.05	2.87
26	0	0	0	0	4.45	3.18
27	0	0	0	0	2.01	2.64
28	0	0	0	0	2.57	2.92
29	0	0	0	0	2.03	2.75
30	0	0	0	0	2.21	3.17

The results of analysis of variance (ANOVA) for grain loss rate of millet are shown in Table 5.

Table 5

Variance analysis of loss rate

Source of error	Sum of square	Free degree	Mean square	*F*	*P*
Model	1336.5	14	95.46	39.38	< 0.0001
x_1	21.7	1	21.7	8.95	0.0091
x_2	58.22	1	58.22	24.01	0.0002
x_3	73.01	1	73.01	30.11	< 0.0001
x_4	139.3	1	139.3	57.45	< 0.0001
x_1x_2	12.46	1	12.46	5.14	0.0386
x_1x_3	0.012	1	0.012	0.005	0.9446
x_1x_4	2.5×10-5	1	2.5×10-5	1.0×10-5	0.9975
x_2x_3	54.54	1	54.54	22.49	0.0003
x_2x_4	49.7	1	49.7	20.5	0.0004
x_3x_4	20.7	1	20.7	8.54	0.0105
x_1^2	109.14	1	109.14	45.02	< 0.0001
x_2^2	828.52	1	828.52	341.73	< 0.0001

Source of error	Sum of square	Free degree	Mean square	*F*	*P*
x_3^2	113.7	1	113.7	46.9	< 0.0001
x_4^2	52.22	1	52.22	21.54	0.0003
Residual	36.37	15	2.42		
Lack of fit	31.83	10	3.18	3.51	0.0893
Error	4.54	5	0.91		
Total	1372.87	29			

The regression model P-value is less than 0.01, which indicates that the regression model is highly significant, and the loss of fit test P-value is greater than 0.05, which indicates that it is not significant, which means that the regression model is well fitted. The significance of the effect of each test factor, interaction term and squared term on the loss rate was analyzed. x_1, x_2, x_3, x_4, x_2x_3, x_2x_4, x_4^2, x_2^2, x_2^2, x_4^2 had highly significant effect, x_1x_2, x_3x_4 had significant effect, x_1x_3, x_1x_4 had insignificant effect. Excluding the insignificant terms, the loss rate regression model equation was developed as follows:

$$Y_1 = +2.55 - 0.95X_1 + 1.56X_2 + 1.74X_3 + 2.41X_4 - 0.88X_1X_2 + 1.85X_2X_3 + 1.76X_2X_4 + 1.14X_3X_4 + 1.99X_1^2 + 5.50X_2^2 + 2.04X_3^2 + 1.38X_4^2 \quad (4)$$

The analysis of variance (ANOVA) for impurity content is shown in Table 6.

Table 6

Variance analysis of impurity rate

Source of error	Sum of square	Free degree	Mean square	*F*	*P*
Model	2049.87	14	146.42	1444.61	< 0.0001
x_1	1.83	1	1.83	18.02	0.0007
x_2	823.92	1	823.92	8128.97	< 0.0001
x_3	13.86	1	13.86	136.77	< 0.0001
x_4	15.68	1	15.68	154.72	< 0.0001
x_1x_2	0.24	1	0.24	2.37	0.1446
x_1x_3	0.17	1	0.17	1.7	0.212
x_1x_4	0.73	1	0.73	7.21	0.0169
x_2x_3	3.6×10-3	1	3.6×10-3	0.036	0.853
x_2x_4	0.81	1	0.81	7.99	0.0127
x_3x_4	4.14	1	4.14	40.86	< 0.0001
x_1^2	170	1	170	1677.29	< 0.0001
x_2^2	1026.76	1	1026.76	10130.29	< 0.0001
x_3^2	213.63	1	213.63	2107.77	< 0.0001
x_4^2	77.72	1	77.72	766.82	< 0.0001
Residual	1.52	15	0.1		
Lack of fit	1.28	10	0.13	2.67	0.1451
Error	0.24	5	0.048		
Total	2051.39	29			

The significance of the effect of each test factor, interaction term, and squared term on impurity rate was analyzed. x_1, x_2, x_3, x_4, x_3x_4, x_2^2, x_2^2, x_3^2, and x_4^2 had highly significant effects, x_1x_2, x_1x_3, x_1x_4, and x_2x_4 had significant effects, and x_2x_3 had nonsignificant effects. Excluding the insignificant terms, the impurity rate regression model equation was developed as follows:

$$Y_2 = 4.63 - 0.28X_1 - 5.86X_2 + 0.76X_3 + 0.81X_4 - 0.12X_1X_2 - 0.21X_1X_4 + 0.23X_2X_4 + 0.51X_3X_4 + 2.49X_1^2 + 6.12X_2^2 + 2.79X_3^2 + 1.68X_4^2 \quad (5)$$

Parameter optimization

In order to obtain the optimal parameter combinations for the operating performance of the cleaning device, the regression equations of loss rate and impurity content were analyzed in combination with the boundary conditions of the test factors, and the lowest loss rate and the lowest impurity content were searched for within the range of the factors, so as to set up a mathematical model for the optimization of the parameters.

$$\begin{cases} s.t. \begin{bmatrix} 15\text{mm} \le x_1 \le 35\text{mm} \\ 200\text{mm} \le x_2 \le 640\text{mm} \\ 420\text{r/min} \le x_3 \le 780\text{r/min} \\ 500\text{r/min} \le x_4 \le 900\text{r/min} \end{bmatrix} \\ \min \quad Y_1, Y_2 \end{cases} \quad (6)$$

The optimum performance of the cleaning device was derived from the optimization solution when the amplitude was 25.75 mm, the length of the stepped jitter plate was 447.92 mm, the crank speed was 580.79 rpm, and the fan shaft speed was 645.49 rpm. Under this parameter combination, the theoretical optimum loss rate was 2.58% and the impurity content rate was 3.61%.

Optimized parameter validation test

To verify the cleaning performance of the optimal parameter combination and to validate the accuracy of the optimization model, verification tests were conducted with the following parameters: vibrating screen amplitude of 26 mm, stepped jitter plate length of 450 mm, crank rotational speed of 580 rpm, and fan shaft rotational speed of 645 rpm. Each test was repeated three times, and the average value of the results was taken as the final verification outcome. The test results are presented in Table 7.

Table 7

Validation test results

Number	Loss rate Y_1 (%)	Impurity *rate* Y_2 (%)
1	2.69	3.88
2	2.56	4.03
3	2.78	3.94
Average	2.68	3.95

The results of the validation test showed that under the optimal parameter combination, the grain loss rate of the millet cleaning device was 2.68%, and the impurity content rate was 3.95%. The optimized parameter combination achieved a superior cleaning effect, indicating that the parameter optimization was effective.

Wrap loss verification test

To quantitatively analyze coercive loss and collect the missed grains at the end of the cleaning process, a PS-20 air-blowing suspension velocity measurement device was used to observe whether grains became suspended at the optimized cleaning airflow velocity. If the grains did not become suspended, it indicated that the loss was not related to the cleaning airflow velocity but was instead caused by the coercive action of residual materials during the cleaning and separation process. Based on this method, the masses of unsuspended and suspended grains among the lost grains were measured, and their proportions in the total grain loss were calculated. The unsuspended grain rate was denoted as W_1, and the suspended grain rate as W_2. When W_1 accounted for a large proportion of the total grain loss, it indicated that coercive loss during the cleaning and separation process was more severe.

To validate the fan speed control variables and to select the optimal combination of fan operating parameters, all fan shaft speeds x_4 were set to 645 rpm. The experimental program and results are presented in Table 8 and Fig. 15. Among these, the sixth group of test parameters represents the optimal parameter combination derived from the regression model optimization and is considered the control group.

Table 8

Validation test results

Number	Amplitude x_1(mm)	Plate length x_2(mm)	Crank speed x_3 (r·min^{-1})	Fan shaft speed x_4 (r·min^{-1})	Loss rate Y_1 (%)	W_1 (%)	W_2 (%)
1	15	200	420	645	15.7	84.9	15.1
2	20	310	510	645	8.58	71.4	28.6
3	25	420	600	645	3.95	40.3	59.7
4	30	530	690	645	7.84	69.3	30.7
5	35	640	780	645	9.61	75.2	24.8
6	26	370	523	645	2.68	18.5	81.5

The coercive loss rates for groups 1-5 in the validation test were calculated to be 13.33%, 6.13%, 1.59%, 5.43%, and 7.23%, respectively. These losses correspond to grains that could not be lifted by the airflow under the test's air-selection conditions, indicating that they could theoretically be separated through the sieve. However, due to the interference of other components on the cleaning sieve, these grains were carried away by the cleaning airflow, resulting in coercive loss. Under the optimal parameter combination in group 6, the proportion of suspended grain loss during cleaning was 81.5%.

According to the statistics, most of the suspended grains belonged to grains that were not full or not fully ripe. The rate of unsuspended grains was the lowest, 18.5%, and the loss rate due to coercion was less than 0.5%. This indicates that the phenomenon of coercion is not easy to occur under this parameter, which verifies the correctness of the method of reducing sorting loss through the Brazil Nut Effect.

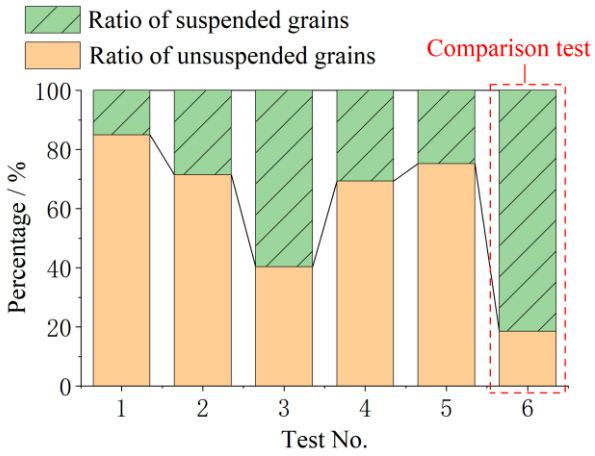

Fig. 15 - The suspension proportion of uncleared grains

CONCLUSIONS

(1) In this study, based on the principle of the Brazil Nut Effect, a numerical simulation of the grain sieving process was conducted using the Discrete Element Method to address the characteristics of light grain mass and small differences in suspension velocity during the cleaning process of the millet threshing mixture. The analysis clarified the structural characteristics of the grain population and identified the main influencing factors that promote efficient grain sieving.

(2) A regression model relating vibration amplitude, stepped jitter plate length, crank rotational speed, and fan shaft rotational speed to cleaning performance was established through bench-scale multifactorial combination tests. This model quantitatively describes the effects of each factor on the grain loss rate and impurity rate.

(3) Based on the regression model and a multi-objective optimization method, the optimal parameter combination was determined to be: vibration amplitude 26 mm, stepped jitter plate length 450 mm, crank rotational speed 580 rpm, and fan shaft rotational speed 645 rpm. Under this parameter combination, the cleaning loss rate was 2.68% (including a wrapping loss below 0.5%) and the impurity rate was 3.95%, confirming the validity and practical effectiveness of the parameter optimization strategy.

ACKNOWLEDGEMENT

This research was supported by the Heilongjiang Provincial Postdoctoral Science Foundation (LBH-Z24251), the Guiding Science and Technology Project of Daqing City (zd-2025-033), the Research Start-up Program for Returned and Introduced Talents (XYB202309), and the "Sanzong" Youth Innovation Talent Program (ZRCQC202304).

REFERENCES

[1] Bao, G., Zhang, Z., Yang, X., Liu, L., Li, J., Lv, Z., & Yang, W. (2024). Design and experiment of separating impurities device for corn plot test harvester based on Coanda effect. *Transactions of the Chinese Society for Agricultural Machinery*, Vol. 55, Issue 10, pp. 234-243.

[2] Cristea, O., Nitu, M., Constantin, G., Munteanu, M., Milea, O., Zaharia, R., & Gradila, M. (2023). Research on the testing of axial flow threshing apparatus for improving their qualitative working indices. *INMATEH Agricultural Engineering*, Vol. 70, Issue 2, pp. 607-614.

[3] Dubey, P., Yogi, J., Kumar, S., Khatoon, S., Kumari, K., & Anand, A. (2024). Shape-dependent size polydispersity: DEM investigation of mixing behavior in a vibrating packed bed system. *Powder Technology*, Vol. 441, pp. 119804.

[4] Guo, H., Guo, L., Li, H., Dong, Y., Zhou, W., & Han, J. (2024). Calibration and experiment of the discrete element simulation parameters for rapeseed stems during the suitable harvest period. *Transactions of the Chinese Society of Agricultural Engineering (Transactions of the CSAE)*, Vol. 40, Issue 24, 20-29.

[5] Hou, H., Cui, Q., Chen, Y., & Chang, Z. (2022). Experiment on air and screen cleaning device of foxtail millet combine harvester. *Agricultural Engineering*, Vol. 12, Issue 8, pp. 93-98.
[6] Hud, V., Lyashuk, O., Hevko, I., Ungureanu, N., Vladut, N., Stashkiv, M., Hevko, O., & Pik, A. (2023). Enhancement of agricultural materials separation efficiency using a multi-purpose screw conveyor-separator. *Agriculture-Basel*, Vol. 13, Issue 4.
[7] Jiang, T., Li, H., Guan, Z., Mu, S., Wu, C., & Zhang, M. (2023). Design and experiments of material uniform dispersion and diversion device on cleaning screen surface for oilseed harvesting. *Transactions of the Chinese Society for Agricultural Machinery*, Vol. 54, Issue 1, pp. 146-158.
[8] Kang, J., Wang, X., Xie, F., Hou, J., Li, Q., & Liu, A. (2025). Design and test of the independently-adjustable concave plate screen for a multi-crop combine harvester. *Transactions of the Chinese Society of Agricultural Engineering (Transactions of the CSAE)*, Vol. 41, Issue 3, pp. 11-21.
[9] Li, M., Yao, Y., Zhu, Y., Li, X., Yue, D., & Geng, D. (2025). Design and experiment of a double longitudinal axial-flow corn threshing device for large feeding capacity. *INMATEH Agricultural Engineering*, Vol. 75, Issue 1, pp. 527-538.
[10] Liu, J., Wang, W., Wang, R., Zhao, L., Chang, L., Yang, W., Zhang, D., Sun, H., & Duan, X. (2022). Nutrition and eating quality of main foxtail millet varieties in China. *Journal of the Cereals and Oils Association*, Vol. 37, Issue 11, pp. 227-235.
[11] Liu, P., Jin, C., Yin, X., Ning, X., & Li, Q. (2019). Research progress of soybean combine harvester cleaning equipment and key technologies. *Acta Agriculturae Zhejiangensis*, Vol. 31, Issue 10, pp. 1758-1766.
[12] Mircea, C., Nenciu, F., Vladut, V., Voicu, G., Gageanu, I., & Cujbescu, D. (2020). Increasing the performance of cylindrical separators for cereal cleaning by using an inner helical coil. *INMATEH Agricultural Engineering*, Vol. 62, Issue 3, pp. 249-258.
[13] Song, L., Wang, L., Feng, X., Wang, H., & Li, Y. (2021). Research status and development analysis of screening devices of grain combine harvester. *Transactions of the Chinese Society for Agricultural Machinery*, Vol. 52, Issue 6, pp. 1-17.
[14] Sun, T., Wu, B., Zhang, H., Han, Y., Liu, H., & Zhang, Y. (2024). Discrete element simulation of particle flow and separation in a vibrating screen with variable rectangular hole screen. *Powder Technology*, Vol. 434, pp. 119305-119317.
[15] Vladut, N., Biris, S., Cârdei, P., Gageanu, I., Cujbescu, D., Ungureanu, N., Popa, L., Perisoara, L., Matei, G., & Teliban, G. (2022). Contributions to the mathematical modeling of the threshing and separation process in an axial flow combine. *Agriculture-Basel*, Vol. 12, Issue 10.
[16] Vladut, N., Ungureanu, N., Biris, S., Voicea, I., Nenciu, F., Gageanu, I., Cujbescu, D., Popa, L., Boruz, S., Matei, G., Ekielski, A., & Teliban, G. (2023). Research on the identification of some optimal threshing and separation regimes in the axial flow apparatus. *Agriculture-Basel*, Vol. 13, Issue 4.
[17] Wang, C., Jin, C., Yang, X., Lei, C., Li, P., & Zhao, Z. (2025). Research status and development trend of screening devices for grain combine harvesters. *Journal of Chinese Agricultural Mechanization*, Vol. 46, Issue 6, pp. 46-54.
[18] Wang, F., Li, B., Zhu, R., Wang, S., Liu, Y., Gao, X., & Yang, X. (2024). Design and test of the wind-sieve type cleaning equipment for cumin threshing machine. *Transactions of the Chinese Society of Agricultural Engineering (Transactions of the CSAE)*, Vol. 40, Issue 22, pp. 39-50.
[19] Wang, F., Alimu, M., Zhang, J., Li, Q., & Xu, L. (2024). Design and experiment of pre-screening cleaning device for combined screen surface of corn grain harvester. *Transactions of the Chinese Society for Agricultural Machinery*, Vol. 55, Issue 5, pp. 135-147+166.
[20] Wang, G., Cao, H., Han, Z., Hao, F., Wu, H., & Su, T. (2014). Analysis of crank connected vibrating-sieve device in corn harvester. *Journal of Agricultural Mechanization Research*, Vol. 36, Issue 1, pp. 65-68+72.